大韓土木學會論文集
第14卷 第2號 · 1994年 3月
pp. 257~268

構 造 工 學

極低荷重사이클을 받는 鋼部材 및 要素의 破壞擧動에 관한 實驗的 硏究

Experimental Study on Failure Behavior of Steel Members and Elements under Very Low Load-Cycles

朴 鍊 洙*
Park, Yeon Soo

Abstract

An experimental study was carried out to elicit important factors causing cracks and rupture of steel members and their elements under imposed large repeated deformations, and of the quantitative relationships among the important physical factors leading to failure. Each of twenty-eight angles and nine thin-plates served as the specimen and was subjected to repeated axial load after undergoing inelastic buckling. Particular attention was paid to the effects of loading pattern, failure mode and cross-sectional shape on the very-low-cycle failure behavior under loading repetitions of the order of a few to twenty. The experimental results show that energy dissipation capacity depends heavily on the entire history of loading, the failure mode, the slenderness ratio and the width-to-thickness ratio. No simple quantitative relations were observed between the initiation of the visible cracks or rupture and the energy dissipation capacity. The maximum values of residual "net" strains are found to range from 25% to 40%, independent of the test parameters.

요 지

강진과 같은 큰 반복하중하에서 강부재 및 그들요소의 균열과 파단에 영향을 미치는 중요한 물리적 인자들을 찾아내어, 그 인자들간의 정량적인 관계를 규명하기 위해 실험적 연구를 수행하였다. 9개의 강판요소와 28개의 앵글 강부재를 시험체로서 사용하였으며, 비탄성 좌굴이 포함된 축방향의 반복하중을 5~20회 정도 받았다. 본 실험은 극저사이클 파괴거동에 있어서 제하이력과 파괴형태 및 단면형상의 영향평가에 특히 촛점을 두었다. 실험결과, 에너지 소산능력은 실험변수에 크게 의존하였으며, 균열의 발생 또는 파단과 에너지 소산능력 사이에 단순한 정량적 관계가 성립되지 않았다. 그러나, 실험변수에 관계없이 균열발생부에 있어서 잔류변형률의 최대치는 일정한 값을 보여주었다.

1. Introduction

Economically-designed steel structures are expected to partially undergo plastic deformation under strong cyclic excitations as in destructive earthquakes. Structural damage and failure are often associated with plastic and/or unstable be-

* 正會員 · 日本 京都大學 防災硏究所 都市耐震센터 공동연구원

havior of thin-walled members due to large cyclic deformations with the initiation of local-buckling. This has motivated the experimental study on failure due to very low-cycles of loading, which are herein meant to involve load repetitions of the order of a few to twenty cycles. This paper presents experimental observations from two tests: one is for thin-plate elements (Test 1) and the other is for angle members (Test 2).

In general, the failure type of structures and their elements may be classified as follows; (1) brittle failure, (2) ductile failure, (3) fatigue failure, (4) creep failure and (5) failure caused by corrosion. Brittle failure is a failure type in structures or elements which usually occurs without prior plastic deformation and at extremely high speed.[1] Ductile failure, however, is preceded by appreciable plastic deformation before actual rupture and finally occurs when displacement reaches a critical value.[2] In fluctuating-load environments, it has been realized that structures and their elements when subjected to repeated loading may fail at stresses or strains below the static strength necessary to start cracking. This type of failure is called fatigue failure.[3]

During an earthquake a bridge or building is subjected to random vibrations caused by the ground motion. In the types of modern construction, the imposed forces must be resisted by the structural frame. When a structural frame is subjected to severe earthquakes, some of the beams and columns undergo substantial inelastic actions and often experience permanent damage. In this case, the failure problem of a structure or its members is correlated with the problem of very-low-cycle loading; combination of relatively small number of load repetitions and large deformations.

In most design of the structural frame for civil engineering structures, namely bridges and buildings, in seismic area, two basic design criteria must be adopted.[4-8] First, a structure and its members should remain within the elastic range against moderate earthquakes, which reasonably may be expected at a structure site during the structure's service life. Second, in extremely large earthquakes, whose possibility of occurrence during the service life of a structure is very low, the structure may be allowed to undergo yield or localized plastic deformation, but not collapse. In seismic design level of conventional structures, however, the extent of the allowable inelastic deformations is a very difficult and nondeterministic problem. The exact prediction, therefore, on the inelastic post-buckling behavior of structures and their members must be essential.

When steel structures and their members are subjected to destructive earthquake motions, the number of load repetitions associated with the significant structural damage may be limited within about 5-20 cycle ranges.[9,10] At that time, since the structures and members partly experience large plastic deformations repeatedly, there is a possibility of structural failure due to a very-low-cycles of loading under load repetitions of the order of a few to twenty cycles. The very-low-cycle loading may result in a ductile failure under repeated excitations rather than fatigue failure. It is necessary to assess exactly the physical aspects of seismic damage and failure for steel members and their elements based on the very-low-cycle failure testing. In order to estimate structural behavior and damage process of steel members and elements for earthquake loading, quantitative investigations through the experiments for steel members and their elements under very-low-cycle loading are performed in this study.

2. Test 1: Plate Elements

The experimental investigations were performed on steel thin-plate specimens with different loading patterns. Special attention is paid to structural failure due to very-low-cycle loading. Three types of failure modes, compression and bending, tension and bending, and pure tension, are involved. The specimen of 6 mm×38 mm rectangular cross section, as in Fig. 1, is chosen to simulate local-buckling and post-buckling behavior of thin-plate elements of structural members. Made of SS400 grade steel, it has the tested length of a thin-plated portion: $l=72$ mm, 18 mm or 9 mm. Observation was made to follow the process of

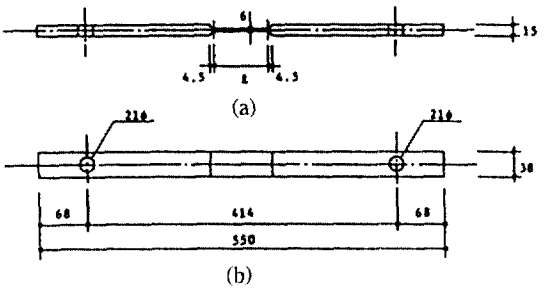

Fig. 1. Test specimen (length in mm).

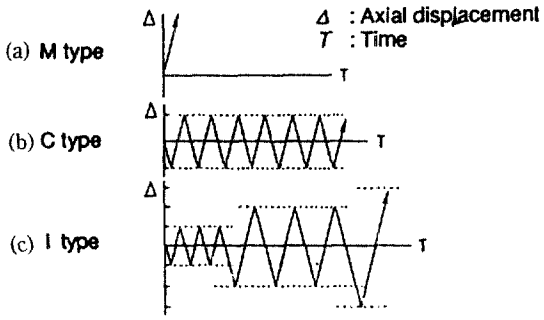

Fig. 2. Fundamental loading patterns.

accumulating damage up to complete failure. This process contains post-buckling deterioration in strength and stiffness, initiation and propagation of cracks, and rupture. Both ends of the specimen were pin-supported. Cyclic uni-axial load was applied to the specimen with the controlled displacement Δ of one end relative to the other, as shown in Fig. 2. Ranges of the ratio Δ/l for each specimen are listed in Table 1.

Typical hysteretic behavior of the specimen is shown schematically in Fig. 3(a) and (b). The ordinate represents the variation of the load P in common, whereas the abscissa indicates the relative axial displacement Δ in (a) and the central deflection V_c in (b). The deflection shapes with predicted plastic-hinges (dark dots) are also shown in Fig. 3(a) together with the directions of load application. The encircled numerals indicate the sequence of load-displacement states. Some examples of P-Δ relationships are shown in Fig. 4. The load and displacement are taken as positive for tension, and are normalized by the yield load N_y, and length l of the thin-portion, respectively. It is observed that failure takes place with one of

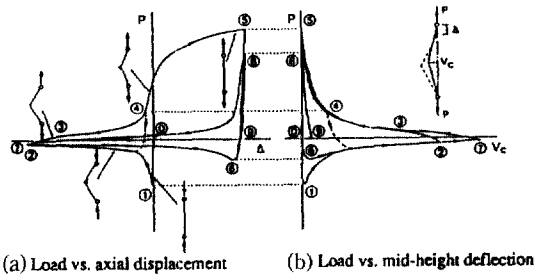

Fig. 3. General behavior of the specimen.

Table 1. Loading patterns

Specimen name	Δ/l	No. of cycles	Type of Failure
L72IS	−0.1∼+0.1	20	
	−0.2∼+0.2	4	
	−0.3∼+0.3	3	
	−0.4∼+0.4	1	TF
L72MT	0 ∼+0.4	1	TF
L72CCA	−1.3∼ 0	3	
	−1.3∼+0.1	3	
	0 ∼+0.2	1	NF*
L72MCA	−1.3∼ 0	1	
	−0.1∼+0.1	3	
	−1.3∼ 0	1	
	0 ∼+0.4	1	TF
L18IC	−0.4∼ 0	3	
	−0.8∼ 0	3	
	−1.6∼ 0	3	
	−3.2∼ 0	2	CF
L18CC	−2.4∼ 0	6	CF
L18CCA	−2.4∼+0.1	4	CF
L09IC	−0.4∼ 0	3	
	−0.8∼ 0	3	
	−1.2∼ 0	3	
	−1.6∼ 0	3	CF
L09MC	−10.4∼ 0	1	CF

*NF: No failure

two modes: very-low-cycle failure due to repetitive combination of compression and bending, and/or tension and bending (compressive/tensile bending failure, CF); and tensile rupture due to

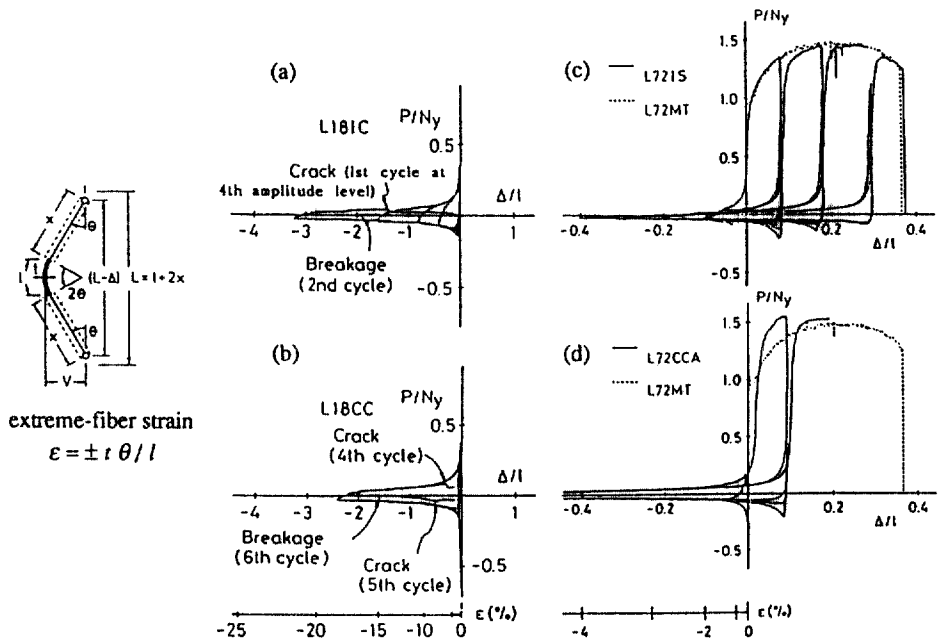

Fig. 4. Load-axial displacement relations.

pure elongation (tensile failure, TF).

In the case of specimen L18IC (Fig. 4(a)) under increased amplitude loading in the contraction side, a crack occurred in the 10th cycle (=the first cycle at the 4th amplitude level) with a sudden decrease of load and the specimen broke in the next cycle. In the case of specimen L18CC (Fig. 4(b)) under constant amplitude loading, cracks occurred in the 4th cycle on the concave side and in the 5th cycle on the convex side, respectively. It is noteworthy that in most cases a crack was initiated from an edge of the concave side when the specimen was stretching. An auxiliary abscissa ε in Fig. 4 indicates the extreme-fiber strain of the thin-portion, calculated on the basis of the assumption that this portion is bent with uniform curvature, as shown in the figure. The failure state, due to the very low-cycle loading with repetitions of the order of several to ten, is strongly related to the maximum strain of the order of 20%, at the extreme-fiber in the cross section.

Specimen L72IS (Fig. 4(c)) was loaded with the increased equal displacement amplitudes in elongation and contraction. Specimen L72MT was stretched monotonically. The maximum displacement on the contraction side in the case of specimen L72CCA (Fig. 4(d)) reached about three times as much as that of L72IS. It is noticed from comparison of the P-Δ relationships that, in some cases, the monotonic tensile load-displacement curve almost provides the envelope for the case of repeated loading (e.g., Fig. 4(c)); whereas in some other cases, those curves do not coincide, since the maximum strengths occur at different deformation stages according to their respective loading histories (e.g., Fig. 4(d)).

Fig. 5 shows some examples of the variation of cumulative energy dissipation E as against the number of cycles f. The energy dissipation is calculated from the area enclosed by the hysteretic load-displacement loops, and is normalized by the maximum elastic strain energy $E_0=\sigma_y^2 Al/(2E_s)$ which can be stored in the tested part of the specimen, where σ_y is the yield stress, A the cross sectional area, and E_s the Young's modulus. The slope of E-f curves depends on the loading histories. In the case of contraction loading (Fig. 5(a)),

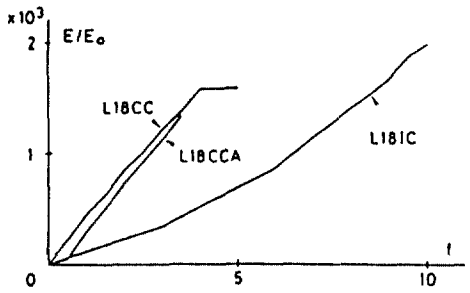

(a) Compressive/tensile bending failure mode

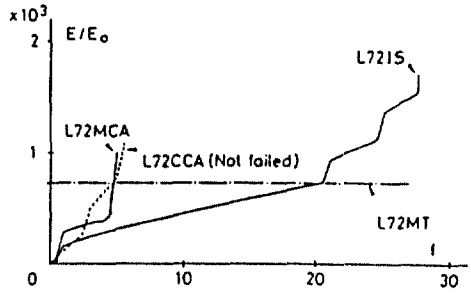

(b) Tensile failure mode

Fig. 5. Energy dissipation in the course of increasing number of cycles.

the energy-increase rates do not change appreciably in the course of loading repetitions; whereas in the case of alternate displacement loading (Fig. 5(b)), those vary abruptly at some stages. The sudden increases of the cumulative energy dissipation are related to the initial cycles at each increased tensile displacement amplitude. Indication may be that the specimen suffers principally in the initial cycles at each amplitude level. The chain line in Fig. 5(b) indicates the energy level at monotonic tensile rupture. There is significant scattering in the total energy dissipation capacity prior to failure. The experimental investigation has revealed that there is a close but not simple relationship between the damage level and the energy dissipation.

3. Test 2: Angles

The Test-1 results for thin-plate elements have shown that the state of ultimate failure under very low-cyclic loading is strongly related to the maximum strain undergone at an extreme-fiber in the cross section. The Test-2 series was performed with special attention to the inelastic post-buckling behavior of steel members and the state of cumulative plastic strains at the critical part of the specimen.

In general, under large compressive and tensile axial loading, load-carrying capacity of members is only related to its respective cross-sectional shapes. However, the nonstationary hysteretic behavior of steel members subjected to severe cyclic loads, which have the cross-sectional shapes such as wide-flanges, angles, and circular and rectangular box tubes, is characterized by the plastic deformations including the local instabilities of thin plates. These local instabilities appear to be a combination of pure elongation and cyclic compressive- and tensile-bending deformations of plate elements in the structural members. So the cracking and rupture of the steel members seem to be related with the accumulation of the pure elongation and local compressive- and tensile-bending deformations.

Steel angles are composed of two simply thin-plates. The angles experience the fundamental failure modes, i.e. failure caused by pure tension, compression and bending, and tension and bending, due to elongation and global bending and local buckling deformations under very-low-cycle loading. Also, by using the steel angles, it is expected that structural factor like the width-to-thickness ratio might be clearly defined and the structural fatigue behavior after global flexural buckling and local buckling might be investigated under the severe cyclic loading. This is a motivation which chosen the steel angle specimens from standard structural shapes. Namely, even though the test specimens in this study are the steel angles, the aim of experiment is to investigate comprehensively the plastic failure behavior of thin-walled steel members under repeated loading rather than that of angles solely. Thus this experiment will provide an useful data to clarify the complicated failure behavior for structural members which are subjected to the fundamental phase such as the pure elongation and the compressive- and tensile-

bending deformations due to repeated loads.

Two types of angles L-40×40×3 and L-40×40×5 of the SS400 grade steel served as specimens. The yield stress and the ultimate tensile strength of the materials are shown in Table 2. A total of 28 specimens, as drawn in Fig. 6, was tested. Each specimen was pin-supported by holding the end plates which were attached by welding perpendicularly to the specimen. The effective length l, being the tested part between the pin-supports, was 318 mm (or 300 mm) or 618 mm, as shown in Fig. 7 and Table 3. Test parameters comprised: (1) slenderness ratio $\lambda=l/i$; (2) width-to-thickness ratio b/t; (3) loading pattern; (4) deflection mode. Here i is the radius of gyration with respect to the v axis of the cross section in Fig. 6(d). The λ value of the specimens ranged 37-41 and 77. The ratio b/t was 8.6 or 13.3-16.4, as shown in Table 3. The choices of (3) were from increasing displacement amplitude (I type), constant displacement amplitude (C type), stepwise varying displacement amplitude (G and S types), and monotonic elongation (M type), in the relative axial displacement Δ, as shown in Fig. 8. The total number of load cycles was set in the loading program up to 16, 24 or 30. The definition of (4) is given in Section 4.1.

A slowly varying uni-axial load was applied to near-centroid G of the cross section (see Fig. 6(d)), using a hydraulic servo-actuator with a loading capacity of 294 kN. A very small eccentricity (about ± 0.5 mm in the u-direction) was given for load to control the deflection mode. Loading was controlled by the relative axial displacement Δ, programmed in the contraction side (L and H series), the elongation side (T series) or in the both sides (A series), as shown in Fig. 8. This causes buckling in the specimen under the initial compressive loading. In order to measure residual local strains after testing, dots were marked on the surface at the both edges and the corner in the cross section, in the direction parallel to the longitudinal axis at intervals of 2mm for a mid-part length of 80mm, using a Vickers hardness tester.

4. Test Results of Angles

Table 2. Mechanical properties of materials

Type	Angle	Yield stress (N/mm^2)	Ultimate strength (N/mm^2)	Elongation (%)
I	L-40×40×3	371	465	31.2
II	L-40×40×3	336	449	29.7
III	L-40×40×5	339	469	27.1
IV	L-40×40×3	331	447	36.7

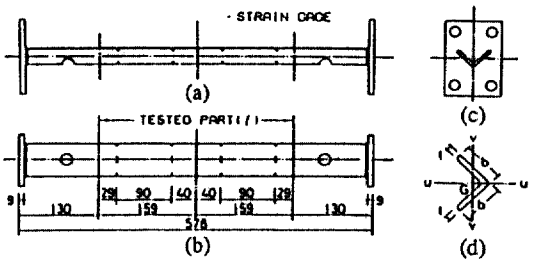

Fig. 6. Test specimen (length in mm).

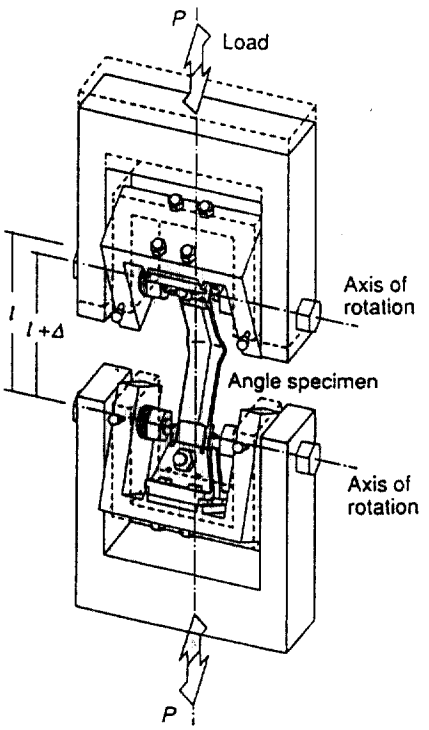

Fig. 7. Specimen supporting system.

Table 3. Specimen sizes and test parameters

Specimen name	Material type	Length l (mm)	Width b (mm)	Thickness t (mm)	Slenderness ratio λ	Width-to-thickness ratio b/t	Loading pattern	Deflection mode
L3IP	I	318	39.6	2.80	40.5	14.1	I	P
L3IN	II	301	40.4	2.55	37.4	15.8	I	N
$L3CP_a$	II	300	40.3	2.55	37.3	15.8	C	P
$L3CP_b$	I	318	39.6	2.83	40.5	14.0	C	P
L3CN	II	301	40.5	2.47	37.4	16.4	C	N
L3GP	I	318	39.5	2.80	40.5	14.1	G	P
L3SP	I	318	39.5	2.82	40.5	14.0	S	P
L3GN	I	318	39.5	2.78	40.5	14.2	G	N
L3SN	I	318	39.6	2.79	40.5	14.2	S	N
L5IP	III	318	39.2	4.56	41.4	8.6	I	P
L5IN	III	300	39.2	4.58	39.0	8.6	I	N
$L5CP_a$	III	317	39.3	4.55	41.2	8.6	C	P
$L5CP_b$	III	317	39.2	4.55	41.2	8.6	C	P
L5CN	III	318	39.2	4.55	41.4	8.6	C	N
H3IP	II	618	40.3	2.49	76.8	16.2	I	P
H3IN	II	618	40.2	2.50	76.8	16.1	I	N
H3CP	II	618	40.3	2.50	76.8	16.1	C	P
H3CN	II	618	40.4	2.50	76.8	16.2	C	N
H3GP	II	618	40.2	2.51	76.8	16.0	G	P
H3SP	II	618	40.4	2.49	76.8	16.2	S	P
T3M	IV	316	39.7	2.97	40.4	13.4	M	–
$T3CP_a$	IV	315	39.6	2.98	40.3	13.3	C	P
$T3CP_b$	IV	316	39.7	2.97	40.4	13.4	C	P
T3CN	IV	318	39.6	2.97	40.7	13.3	C	N
A3CP	IV	316	39.7	2.99	40.4	13.3	C	P
A3CN	IV	315	39.6	2.97	40.3	13.3	C	N
A3IP	IV	316	39.7	2.98	40.4	13.3	I	P
A3IN	IV	315	39.5	2.96	40.3	13.3	I	N

4.1 Buckling and Cracking Behavior

Fig. 9 is a sketch of buckling deformation and visible cracking. The positive (P mode) or negative (N mode) deflection was observed as defined in the figure. The global buckling pattern was accompanied by significant localized deformation due to plate buckling of the legs at the mid-part of the specimen, which induced very large strains. Fig. 10 shows the observed compressive strength in relation to the column curve, where P_{cr} is the buckling load.

Typical examples of the observed load-axial displacement relationships are shown in Fig. 11. The numbers of load cycles at three cracking states

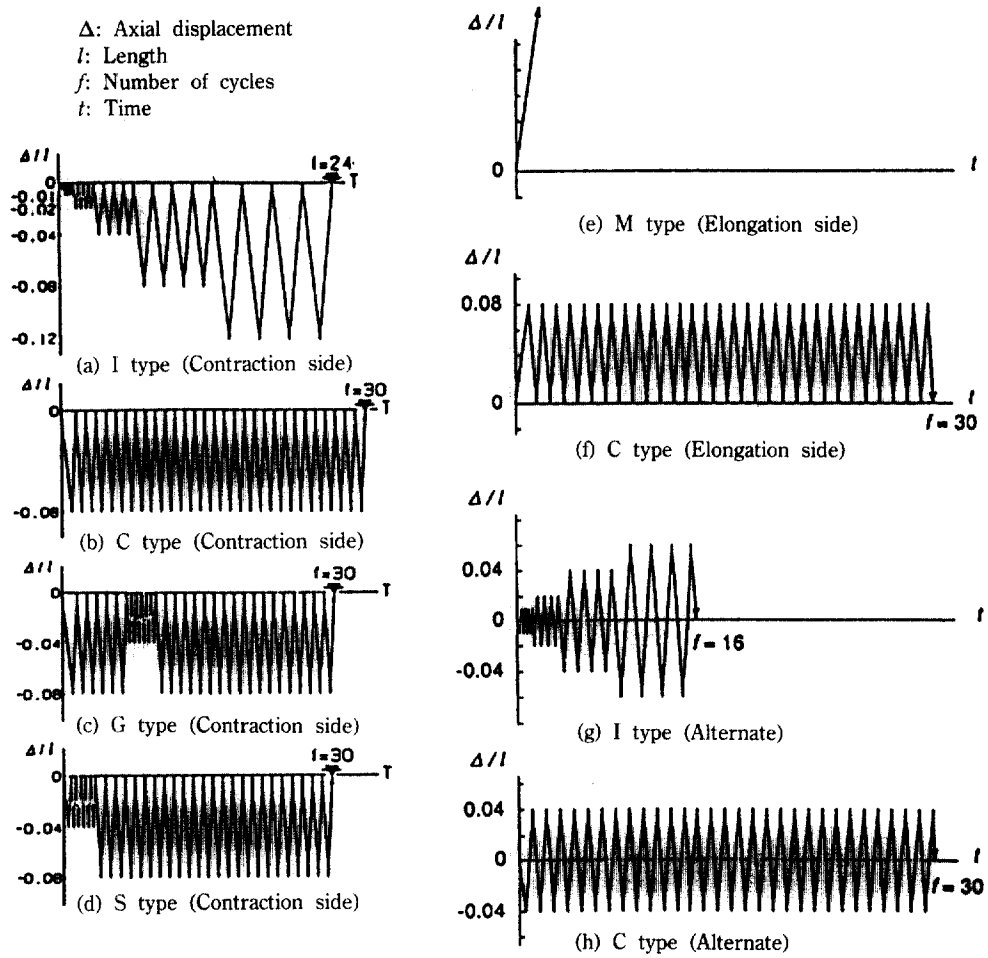

Fig. 8. Loading patterns.

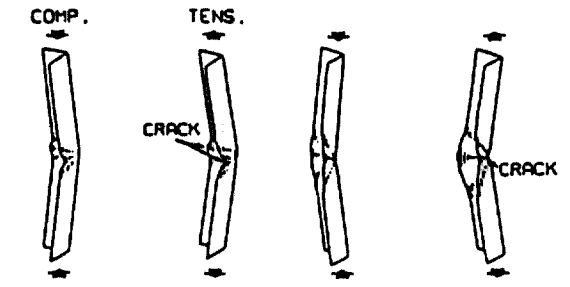

(a) Positive deflection mode (b) Negative deflection mode

Fig. 9. Deflection modes and cracking patterns.

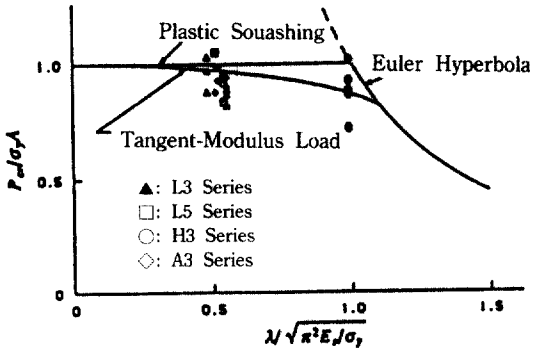

Fig. 10. Column curve and observed strength.

and rupture are shown for each specimen in Table 4. Irrespective of the loading patterns and deflection modes, visible cracks were initiated during stretching on the concave side of the overall buckling deformation (f_{cav}) induced in the preceding load cycles. Visible cracks on the convex side (f_{vex}) were observed within 1-4 cycles following the concave side cracking. Cracking on the concave and convex sides rapidly penetrated through the thickness of the legs (f_{pen}).

In most specimens subjected to the I type loading, no cracks were observed under the repetition of global strain Δ/l less than 8%, but visible cracks appeared in the 1st cycle at the amplitude level of 12% global strain. In the case of the C type loading under 8% global strain, visible cracks occurred during the 4-9th cycle. Inelastic buckling caused a sudden decrease in the compressive load-carrying capacity, but only a slight decrease in the succeeding tensile load-carrying capacity. However, both the compressive and tensile load-carrying capacities were considerably decreased by the initiation of cracking. It is thus found that the outset of failure is closely related to the occurrence of a visible crack. The cracks were quickly enlarged in the course of load repetitions. Sixteen specimens, for which the value f_{rup} is indicated in Table 4, were completely ruptured within the programmed loading cycles. The test results show that f_{rup} decreases as b/t becomes smaller and as λ becomes larger, and is less when given displacement includes elongation for the specimen. This may be because the local deformation of the angle was severely concentrated in these cases.

A pair of specimens whose names contain "a" or "b", in Tables 3 and 4, were subjected to the same loading condition. The three sets of identical angles showed very similar load-displacement curves and completely ruptured in the identical number of cycles, indicating the trustworthiness of this series of test.

4.2 Energy Dissipation Behavior

The relationships between the dissipated energy E and the number of cycles f are shown in Fig. 12. In the cases of the same loading pattern

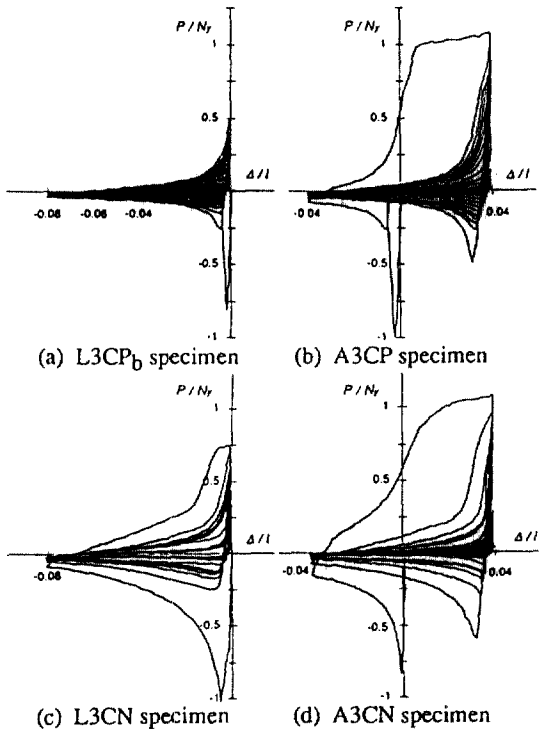

Fig. 11. Load-axial displacement relations.

and the same deflection mode, very similar processes of energy dissipation were observed (see curves for L5CPa and L5CPb, and L3CPa and L3CPb in Fig. 12(b)). If deflection modes are different, however, energy dissipation behavior is quite different even among specimens under the same loading pattern (see Figs. 12 (a) and (b)); the P-Δ curves in the case of the positive deflection mode show thinner hysteresis loops than the negative deflection mode (for example, compare (a) and (b) with (c) and (d), respectively, in Fig. 11). Therefore, the cumulative energy, i.e., the energy dissipation capacity is seen to depend on the deflection mode.

From comparison of three types of loading patterns, C, G and S, the effect of loading sequence is investigated. In the case of the positive deflection mode (see Fig. 12(c)), the number of cycles at rupture f_{rup} becomes small in the order of the C, G and S types of loading, but the energy dissipation capacity is not substantially different among these three types.

Table 4. Test results

Specimen name	Bucking load P_{cr} (kN)	Number of load cycles: Crack f_{cav}	Crack f_{vex}	Crack f_{pen}	Rupture f_{rup}	Dissipated energy E/E_o	Strain at cracked portion: Tens. ε_{tens} (%)	Comp. ε_{comp} (%)
L3IP	71.4	17	18	18	–	131	–	–
L3IN	58.9	20	21	21	–	235	–	–
L3CP$_a$	64.2	9	10	10	–	133	27.5	−29
L3CP$_b$	66.8	5	8	8	23	115	30	−32.5
L3CN	69.0	7	8	8	–	220	–	−41
L3GP	66.0	5	9	10	25	112	27.5	−35
L3SP	69.7	8	12	12	27	122	30	−32.5
L3GN	72.8	6	–	7	–	170	–	−30
L3SN	76.3	10	–	11	–	221	–	−35
L5IP	105.2	21	23	23	–	236	35	−35
L5IN	120.7	22	–	22	–	410	–	−30
L5CP$_a$	96.7	9	12	12	19	211	32.5	−35
L5CP$_b$	109.2	9	12	12	19	214	30	−32.5
L5CN	107.5	9	13	13	21	378	35	−35
H3IP	68.4	18	21	21	–	78	35	−35
H3IN	59.9	18	–	22	–	117	–	−35
H3CP	49.1	5	8	9	17	66	32.5	−35
H3CN	58.3	5	–	8	–	104	–	−35
H3GP	48.6	6	9	11	22	75	30	−35
H3SP	62.7	9	12	12	22	83	35	−35
T3M	–	–	–	–	1	466	[115]*	–
T3CP$_a$	–	4	7	8	17	267	30	−30
T3CP$_b$	–	4	8	8	17	259	35	−30
T3CN	–	6	8	8	–	293	–	−30
A3CP	75.0	4	7	8	17	190	35	−30
A3CN	67.1	4	7	7	20	198	35	−30
A3IP	70.6	8	11	11	13	179	[65]*	−35
A3IN	74.8	12	13	13	14	215	[65]*	−35

*[ ] means local strain due to tensile rupture.

No simple quantitative relations were observed between the initiation of a visible crack or the rupture of a specimen and the energy dissipation capacity. Energy dissipation process and capacity are influenced by the entire history of loading, deflection mode, slenderness ratio and width-to-thickness ratio.

4.3 Local Strain Distributions

Fig. 13 shows typical distributions of residual local strains accumulated at the edges and corners in the cross section after testing. Visible cracks

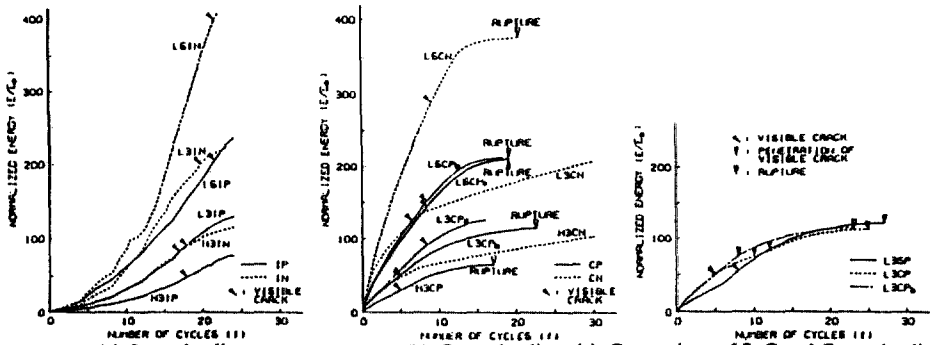

(a) I type loading (b) C type loading (c) Comparison of S, G and C type loadings

Fig. 12. Comparison of energy dissipation in the course of increasing number of cycles.

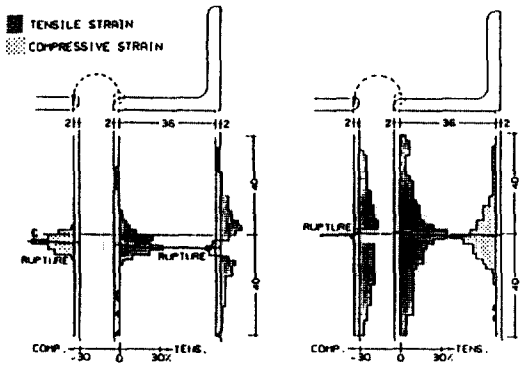

(a) Positive deflection mode (b) Negative deflection mode

Fig. 13. Distribution of local strain in angle test.

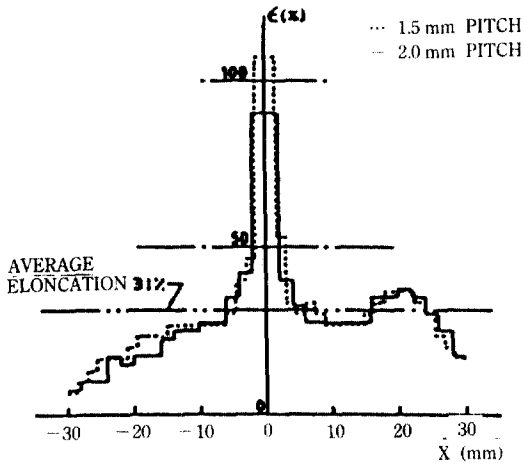

Fig. 14. Distribtuion of local in material test.

are located near thre regions of severe concentration of strains. The maximum absolute value of residual "net" strains, excluding contributions from the crack opening, of all the specimens was in the range of 25-35% on the tensile side and 30-40% on the compressive side (see ε_{tens} and ε_{comp} in Table 4). It does not depend on the loading pattern, delfection mode, slenderness ratio or width-to-thickness ratio. For comparison, Fig. 14 shows the local strain distrbution in the monotonic-tensile material test with a JIS (Japanese Industrial Standard) 13-B type specimen. The maximum "net" strain measured at 1.5 mm or 2 mm intervals near the ruptured portion, which is indicated as the origin of the abscissa, was about 100 %, even though the average elongation of the specimen was about 30%. The residual strain values in the angle tests reflect the effect of repeated loading. Analytical study is under way by means of numerical simulation using the finite element method in relation to these phenomena, especially as to mecahnical behavior and local stress-strain histories.

5. Conclusions

The main conclusions are summarized as follows:

1) The experimental investigation reveals that, regardless of loading patterns and delfection modes, visible cracks were initiated during stretching on the concave side of the overall bending deformation induced in the preceding load cycles.

2) The number of load cycles at rupture decrea-

ses as width-to-thickness ratio becomes smaller, as slenderness ratio becomes larger, and when the loading program includes elongation.

3) The perfect resemblance of very-low-cycle fatigure behavior was observed under the identical loading pattern and deflection mode, indicating the trustworthiness of this experimental investigation.

4) Energy dissipation capacity depends heavily on the entire history of loading, failure mode, slenderness ratio and width-to-thickness ratio. No simple quantitative relations were observed between the initiation of visible cracks or rupture and the energy dissipation capacity.

5) The maximum value of residual "net" strains at the outbreak of a visible crack under very-low-cycles of loading was of the order of 25-40%. It is independent of the loading pattern, failure mode, slenderness ratio and width-to-thickness ratio.

REFERENCES

1. Rolfe, S.T. and Barsom, J.M., *Fracture and Fatigue Control in Structures (Application of Fracture Mechanis)*, Prentices-Hall, Inc., 1977.
2. Caddell, R.M., *Deformation and Fracture of Solids*, Prentice-Hall, Inc., 1980.
3. Miner, M.A., "Cumulative Damage in Fatigue", *Jour. of Applied Mechanics*, 1945, pp. A159-A164.
4. Hanson, R.D., "Comparison of Static and Dynamic Hysteresis Curves", *Jour. of Engineering Mechanics Division*, ASCE, Vol. 92, No. EM5, 1966, pp. 87-113.
5. Bertero, V.V., Popov, E.P., and Krawinkler, H., "Beam-Column Subassemblages under Repeated Loading", *Jour. of Structural Division*, ASCE, Vol. 98, No. ST5, 1972, pp. 1137-1159.
6. *Earthquake Resistant Regulations-A World List*, International Association for Earthquake Engineering, Tokyo, Japan, 1984.
7. *Guidelines to Structural Calculation under the Building Standard Law*, The Building Cener of Japan, 1991 (in Japanese).
8. *Elasto-Plastic Behavior and Seismic Design of Steel Structures*, Japan Society of Civil Engineers, Osaka, Japan, 1993 (in Japanese).
9. Nonaka, T. and Iwai, S., "Failure of Bar Structures under Repeated Loading", *Structural Failure* (edited by T. Wierzbicki and N. Jones, John Wiley & Sons), 1988, pp. 389-433.
10. Iwai, S. and Nonaka, T., "Plastic Fatigue of Structural Members under Repeated Loading-Survey and Recent Developments", *Annuals of Disaster Prevention Research Institute*, Kyoto University, No. 31B-1, 1988, pp. 89-104 (in Japanese).

(接受 : 1993. 10. 4)